32

TECHNICAL NOTE

D-1503

HEAT TRANSFER AND PRESSURE DISTRIBUTIONS ON A

HEMISPHERE-CYLINDER AND A BLUFF-AFTERBODY MODEL

IN METHANE-AIR COMBUSTION PRODUCTS AND IN AIR

By Irving Weinstein

Langley Research Center
Langley Station, Hampton, Va.

NATIONAL AERONAUTICS AND SPACE ADMINISTRATION

WASHINGTON   December 1962

NATIONAL AERONAUTICS AND SPACE ADMINISTRATION

TECHNICAL NOTE D-1503

HEAT TRANSFER AND PRESSURE DISTRIBUTIONS ON A

HEMISPHERE-CYLINDER AND A BLUFF-AFTERBODY MODEL

IN METHANE-AIR COMBUSTION PRODUCTS AND IN AIR

By Irving Weinstein

SUMMARY

An experimental investigation has been made to indicate the validity of using methane-air combustion products as the test medium for aerodynamic heating and loading tests. Tests were conducted on a hemisphere-cylinder and on a bluff-afterbody model, both in methane-air combustion products and in air alone, and covered a range of Mach numbers from 6 to 9, total temperatures from approximately 2,000° F to 3,100° F, and stream Reynolds numbers per foot from 0.45×10^6 to 2.8×10^6.

The data showed that the nondimensional heating-rate distribution along a hemisphere-cylinder as obtained in combustion products was in good agreement with that obtained in air, and the results were in reasonable agreement with theory. The stagnation-point heating rates in air and in combustion products over the hemisphere-cylinder agreed within 10 percent of the theoretical values. The pressure distributions around a hemisphere-cylinder obtained from tests in combustion products were in good agreement with those obtained in air and could be predicted by Newtonian flow theory. The tests in combustion products of a bluff-afterbody model produced nondimensional heat-transfer coefficients which were in fair agreement with results obtained in air.

INTRODUCTION

With the advent of manned hypersonic flight there is a great need for large-scale ground test facilities capable of true flight simulation at hypersonic speeds. Such facilities permit research testing of full-scale components of vehicles under realistic combinations of aerodynamic heating and loading. The power requirements for producing the required test stream energy levels at the desired large flow rates of air for these large facilities are prohibitive. Consequently, other methods must be utilized to obtain the desired simulation. One such method consists of burning a fuel in air and expanding the combustion gases through a nozzle and using these combustion products as the test medium, in which case the aerodynamic heating and loading may be different from that experienced by a body in flight. Hence, the difference in heating and loading

resulting from testing in combustion products rather than in air must be evaluated.

This paper presents the results of an experimental investigation wherein the actual heating and loading distributions on two simple bodies were measured at hypersonic velocities in combustion products and in air. One of the bodies was a hemisphere-cylinder used to measure local heating rates and pressure distributions; the other was a bluff-afterbody configuration used for comparison of heating rates over areas washed by wakes. Comparison of the test results was made to indicate the measured differences in nondimensional heating and loading afforded by the two test media. Heat-transfer and pressure-distribution data obtained in combustion products are also presented for the bluff-afterbody shape at angles of attack of approximately 0° and 9.5° as a further interest in areas washed by wakes. The hemisphere-cylinder-model data were compared with theory.

The tests in combustion products were conducted in the 7-inch Mach 7 pilot tunnel at Langley Research Center. This facility is a combustion-process tunnel which develops Mach numbers from about 7 to 9 depending upon the stagnation temperature and pressure and the nozzle throat area. Data were obtained in this tunnel at stream Reynolds numbers per foot between 0.45×10^6 and 1.1×10^6, at model stagnation pressures from approximately 4 to 14 psia, and at stagnation temperatures between $2,100^\circ$ F and $3,100^\circ$ F.

The tests in air were conducted in the Langley 11-inch ceramic-heated tunnel, a Mach 6 facility which achieves the required energy level through use of a ceramic storage-type heat exchanger. Data were obtained at a stream Reynolds number per foot from 1.6×10^6 to 2.8×10^6, at model stagnation pressures from approximately 14 to 17 psia, and at stagnation temperatures from $2,000^\circ$ F to $2,750^\circ$ F.

SYMBOLS

c   specific heat, $\dfrac{Btu}{lb\text{-}^\circ R}$

c_p specific heat at constant pressure, $\dfrac{Btu}{lb\text{-}^\circ R}$

C_p pressure coefficient based on free-stream conditions, $\dfrac{p_l - p_\infty}{q_\infty}$

D   maximum diameter of bluff-afterbody model, in.

h   heat-transfer coefficient, $\dfrac{Btu}{ft^2\text{-}sec\text{-}^\circ R}$

k   thermal conductivity, $\dfrac{Btu}{ft\text{-}sec\text{-}^\circ R}$

M   Mach number

2

N_{Pr} Prandtl number, $\dfrac{c_p\mu}{k}$

N_{St} Stanton number, $\dfrac{h}{\rho V c_p}$

p pressure, psia

q_c convective heating rate, $\dfrac{Btu}{ft^2\text{-sec}}$

q dynamic pressure, lb/sq ft

r nose radius, in.

s distance along meridian profile of body, measured from points indicated in figures, in.

T temperature, ^{o}R (unless otherwise indicated)

t model wall thickness, ft

V velocity, ft/sec

x distance aft of maximum diameter, measured parallel to model center line, in.

α angle of attack, deg

β meridian angle, deg

θ angle from stagnation point on hemisphere, deg

ρ density, lb/cu ft

τ time, sec

μ viscosity, lb/ft-sec

Subscripts:

aw   adiabatic wall condition

o   initial

l local condition

m   model

s   stagnation point

t   total

w   wall condition

∞   free-stream condition

MODELS

Two different model configurations were tested, a hemisphere-cylinder and an irregular-shaped model. The irregular-shaped model had a blunt face with an afterbody which had a rapid reduction in size aft of the maximum diameter. This model will hereafter be referred to in the text as a bluff-afterbody model. Separate models of each configuration were constructed for heat-transfer and for pressure-distribution tests.

Hemisphere-Cylinder Models

Heat-transfer models.- Two similar hemisphere-cylinder heat-transfer models were constructed, one for testing in combustion products and the other for testing in air. Figure 1(a) shows a cross-sectional view of one of these heat-transfer models. These models were about 3 inches long with a 0.75-inch nose radius and had a uniform wall thickness of 0.026 inch. The models were machined from 309 stainless steel which, of the materials available, had the highest resistance to scaling with a scaling temperature of approximately 2,000° F. The models were instrumented with 15 thermocouples of No. 30 gage chromel-alumel wire tack-welded to the inside wall in one longitudinal plane in the positions shown in figure 1(a). The outer surfaces of the models were polished to a finish corresponding to approximately 8 microinches rms and were wiped clean between runs. The finish was approximately 40 microinches rms at the conclusion of the tests. These measured values are the maximum variations over the surface obtained with the use of a profilometer and a diamond-point stylus.

Pressure-distribution model.- The pressure-distribution model had the same external geometry as the heat-transfer models with the exception of a 0.1-inch difference in length. This model had a wall thickness of 0.25 inch and had 15 pressure orifices located in a spiral pattern as shown in figure 1(b). The pressure orifices were installed by brazing 0.020-inch inside-diameter tubing in the model wall and were then made flush with the surface. The pressure transducers used for this test were of the strain-gage type, with ±10- and ±15-psi gages used over the major portion of the hemisphere and 0- to 1-psia gages used near the rear of the hemisphere and on the cylindrical portion of the model. Figure 2 shows a photograph of one of the two heat-transfer models and of the pressure-distribution model. Most of the 0.020-inch inside-diameter pressure orifices may be seen in the photograph. The model finish does not appear typical since a dulling spray was used for photographic purposes to cut down on light reflection. This model was later reinstrumented with 0.040-inch inside-diameter tubing before the test in air in order to reduce the test time required to stabilize the pressures on the cylindrical portion of the model.

Bluff-Afterbody Models

Heat-transfer model.- The heat-transfer model for the bluff-afterbody configuration is shown in the photograph of figure 3, taken after completion of the tests. The forward portion of the model had a conical shape with a 0.5-inch nose radius and was made of boron nitride, which effectively insulated the instrumented afterbody from any large heat sink. The afterbody was made of 347 stainless steel and had a wall thickness which varied from 0.010 to 0.011 inch and had a maximum surface roughness of 8 microinches rms. Twenty-one thermocouples of No. 30 gage chromel-alumel wire were tack-welded to the inside surface in a longitudinal plane as shown in figure 4(a). Also shown are some pertinent dimensions and a table of measured wall thicknesses at the various thermocouple locations. The model afterbody was insulated from the sting of the model with boron nitride which has a low thermal conductivity. This insulation completely isolated the afterbody from any contact with a material having a high conductivity.

Pressure-distribution model.- A cross section of the pressure-distribution model of the bluff-afterbody configuration is presented as figure 4(b). Included in the figure is a table of the pressure-orifice locations. This model was constructed to the same external dimensions as the heat-transfer model but had a wall thickness at the stagnation point of 0.75 inch and a wall thickness along the afterbody which varied from 0.1 to 0.2 inch. There were 12 orifices of 0.040-inch inside-diameter stainless-steel tubing brazed into the model wall in a longitudinal plane as shown in the figure. Strain-gage-type pressure transducers to measure the pressure outputs over ranges of 0 to 1 and 0 to 2 psia were used for the tests of this model. The entire model was made of 347 stainless steel.

FACILITIES AND TESTS

The tests using the combustion products formed from the burning of methane in air as the test medium were made in the 7-inch Mach 7 pilot tunnel at Langley Research Center. The tests in air alone were conducted in the Langley 11-inch ceramic-heated tunnel.

Apparatus

7-inch Mach 7 pilot tunnel at Langley Research Center.- The 7-inch Mach 7 pilot tunnel at Langley Research Center is a hypersonic blowdown facility with a high-energy level obtained by burning a mixture of methane and air under high pressure, with the combustion products serving as the test medium to obtain hypersonic flight simulation. A drawing of a portion of this tunnel is shown in figure 5. Air is introduced at pressures up to 2,300 psia, then mixed with the methane, and burned in the combustion chamber. The combustion products are then expanded through an axisymmetric nozzle and pass through the free-jet test section. The flow is then diffused in a straight-tube diffuser and pumped to the atmosphere by means of a single-stage annular air ejector, not shown in the drawing.

The nozzle throat temperature is controlled by injecting and regulating a film of cold air along the nozzle inner surface just upstream of the throat. Tunnel stagnation temperatures are obtained by recording the output of four iridium-iridium 40-percent rhodium thermocouples located near the downstream end of the combustion tube at various radial positions. The stagnation temperature is controlled by regulating the fuel-air ratio. Diametrical pitot-pressure surveys and stagnation-temperature surveys made over the length of the test region indicate a usable test core diameter of between 2.5 and 3.0 inches, dependent upon pressure. Over this diameter of the test core there is a ±2-percent variation in pitot pressure and in total temperature (which corresponds to a maximum variation in Mach number of ±0.07).

For a given test run, the flow is started and allowed to reach the desired equilibrium conditions. The model is then injected into the stream by means of an hydraulically actuated mechanism which requires approximately one-fourth second to position the model for testing. The model can then be removed from the test section at the desired time. A photograph of a hemisphere-cylinder model in test position in the tunnel test section is shown as figure 6.

Langley 11-inch ceramic-heated tunnel.- The tests conducted in air were made in the Langley 11-inch ceramic-heated tunnel. The ceramic heater consists of a large vertical pressure chamber which is lined with zirconia brick near the top and alumina brick near the bottom. The bricks are arranged and sealed in such a way that the airflow cannot escape through the joints between the bricks. The 28-inch-diameter pebble bed consists of a 6-foot depth of 3/8-inch-diameter alumina spheres at the base with a 14-foot depth of 3/8-inch-diameter zirconia spheres on top.

Prior to a test, the pebble bed is heated with the combustion products of propane and air which are forced down through the bed and exhausted at the base. When the bed has reached the desired temperature, the burner is turned off and air is then forced upward through the bed. The air picks up the heat from the hot pebbles as it rises through the bed and emerges at a temperature approximately equal to the surface temperature of the bed. The air is then expanded through a nozzle to the test section and discharged to the atmosphere. The nozzle used for the present tests was an 8° semiangle conical nozzle which had a geometric area ratio of exit cross-sectional area to throat cross-sectional area of 75 and developed a nozzle-exit Mach number of approximately 6.1 near the center line. Preliminary pitot-pressure surveys indicated a usable test core of approximately 8 inches. In the present case the model was tested with its center line about $1\frac{3}{4}$ inches off the nozzle center line in order to minimize the model surface pitting caused by ceramic dust picked up from the heat exchanger. The average flow angularity resulting from off-axis testing in the conical flow was about 2°. The model was programed into and out of the test stream at the desired time after tunnel equilibrium conditions were reached. This test facility is described in more detail in reference 1.

Test Procedure

Three different nozzle throat sizes used during the period of these tests, along with the temperatures and pressures covered, gave a Mach number range from about 7 to 9 in combustion products. The stream Reynolds numbers per foot obtained from the tests in combustion products ranged from 0.45×10^6 to 1.1×10^6. The model stagnation-point pressures varied from about 4 to 14 psia, and the stagnation temperature ranged from approximately $2,100^\circ$ F to $3,100^\circ$ F.

The tests in air were conducted at a nominal Mach number of 6, at stream Reynolds numbers per foot of 1.6×10^6 to 2.8×10^6, at model stagnation pressures between 14 and 17 psia, and at stagnation temperatures from $2,000^\circ$ F to $2,750^\circ$ F.

During each test run, the tunnel stagnation conditions were established before the model was subjected to the stream. The model was then inserted into the stream rapidly so as to give it, as nearly as possible, a step-function exposure to stream-flow conditions. For the bluff-afterbody model tested at angle of attack, the model was preset at the desired angle before injection into the flow. The length of each of the tests for the heat-transfer models ranged from about 4 to 8 seconds. The pressure-distribution models were kept in the flow for approximately 20 to 30 seconds. The outputs from the thermocouples and pressure transducers used for measuring the local temperatures and pressures on the models were recorded on oscillographs. The records were in the form of continuous traces where the calibrated deflection from a given reference represents the temperature or pressure at any given time. The thermocouple reference junctions were maintained at the local ambient temperature.

Accuracy

The model quantities measured are estimated to be accurate within the following limitations:

Angle of attack, deg . . . . ± 0.1
Wall thickness of heat-transfer model, in. . . . . ± 0.005
Free-stream Mach number . . . . ± 0.05
Temperature, $^\circ$R . . . . ± 25
Time, sec . . . . ± 0.03
Pressure, psi . . . . ± 0.05

DATA REDUCTION

The heat-transfer data were reduced by first converting the outputs of the thermocouples to temperatures and then plotting them as functions of time. Temperature-time curves for five of the thermocouple locations for a typical test run are presented as figure 7. Figure 8 shows the temperature distribution along the hemisphere-cylinder model at several increments of time. Maximum heat-transfer rates were desired, which would occur when the wall was still cool, that

is, at the earliest time after the starting transients were considered negligible
and when the enthalpy potential across the boundary layer was a maximum. After
the model was inserted into the flow, only about 0.2 second was required to over-
come the initial temperature lag due to the starting transients as may be seen in
figure 7. A similar method for obtaining the rate of heat flow into a hemisphere-
cylinder model is described in references 2 and 3. Local film heat-transfer
coefficients were determined by using the one-dimensional transient-heat-flow
equation such that

$$h = \frac{\rho_m c_m t \dfrac{dT_w}{d\tau}}{T_{aw} - T_w}$$

where $dT_w/d\tau$ represents the slope of a temperature-time curve at a given time.
The model was assumed to have a negligible temperature gradient through the wall
and a negligible lateral or longitudinal heat flow. Losses due to radiation
from the model were also negligible since the heating rates were measured near
the start of the test when the wall was still relatively cool.

The slopes of the temperature curves at several times during the first 2
or 3 seconds of heating were plotted against the difference between the adiabatic
wall temperature and actual wall temperature, as shown in figure 9. The points
which fall below the lines on the right side of figure 9 represent the data
obtained during the time interval when the starting transients were present and
therefore may be neglected. The next several points to the left of these repre-
sent the desired transient heating when the conduction and radiation are negli-
gible so that the slope of a straight line from the origin through these points
can be considered to be proportional to the desired maximum local heating rate.
The group of points to the far left were obtained at times beyond the initial
heating where calculations show that conduction and radiation have a large effect,
and were consequently neglected. The heat-transfer rates were then determined
from the relation $q_c = h\left(T_{aw} - T_w\right)$. The adiabatic wall temperatures used to
reduce the heat-transfer data were computed from the equation

$$T_{aw} = \eta_r\left(T_s - T_l\right) + T_l$$

where $\eta_r = N_{Pr}^{1/2}$ is the recovery factor for laminar flow. In the reduction
of data obtained in combustion products, the thermal and transport properties
used for methane-air combustion products were obtained from reference 4. The
values of T_l were obtained from the measured stagnation temperatures and pres-
sures and the computed Newtonian pressure distributions around the body.

The temperature-time curves for the bluff-afterbody configuration showed an
initial temperature lag over the first 0.3 second. The heating rates for these
models were obtained directly by measuring the slopes of the temperature-time
curves since, after the initial temperature lag, the slopes were reasonably linear
and could be measured fairly accurately. These slopes were obtained for a time
corresponding to 0.35 second after injection into the flow. Since the adiabatic

wall temperatures were not readily obtainable for this model, the stagnation temperatures were used to compute the Stanton numbers.

The pressure models were kept in the stream longer than the heat-transfer models in order that the pressures could be stabilized as completely as possible. The pressure distributions obtained in this manner, therefore, correspond to equilibrium flow about the body and were obtained from the transducer outputs near the end of each test.

RESULTS AND DISCUSSION

Hemisphere-Cylinder Models

Heat transfer.- A summary of the pertinent experimental stagnation-point heat-transfer data for the hemisphere-cylinder models is presented in table I. The heat-transfer coefficients and heating rates listed were determined by the method described in the previous section. Theoretical heating rates for comparison with these data were computed by the method of reference 5 and are compared with the experimental values in figure 10. The solid line in this figure represents the condition where experiment and theory are equal, and the dashed lines indicate a 10-percent variation with theory. The data, in general, fall within these limits and are considered to be well within the accuracy generally experienced from similar heat-transfer tests.

The experimental heat-transfer distribution along the hemisphere-cylinder is plotted in figure 11 as a ratio of the local heat-transfer rate to that at the stagnation point for the two tests in air and for two typical test runs in the combustion products. The nondimensional heating-rate distribution obtained in combustion products is seen to be in rather good agreement with that obtained in air alone. The theoretical curve was obtained by the method used in reference 6 which calculates directly the dimensionless heat-transfer distribution $q_{c,l}/q_{c,s}$

around the hemisphere. The value of the ratio along the cylinder was considered to be equal to the computed value at the hemisphere-cylinder juncture. Although theory appears to be slightly higher than experiment over the hemisphere and lower than experiment at the hemisphere-cylinder juncture, there is reasonably good agreement between experiment and theory along the body surface.

Pressure distribution.- The nondimensional pressure distribution around the hemisphere-cylinder model is plotted in figure 12 for the tests in combustion products and in air. A theoretical curve is shown which was computed from the modified theory for Newtonian flow. These pressure distributions show that the results obtained from combustion products are in good agreement with those obtained in air and could be predicted satisfactorily by Newtonian flow theory. However, the combustion-products data for the cylinder appear high as a result of the long lag time required for stabilizing the pressure in the 0.020-inch inside-diameter pressure tubing. The pressures on the cylinder during a test run were of the order of 0.01 atmosphere. Before the test in the Langley 11-inch ceramic-heated tunnel, all pressure orifices were closed and new holes drilled where possible for 0.040-inch inside-diameter tubing diametrically opposite the

9

original holes. Because of the brazing of the original tubing, which was difficult to redrill, there was no stagnation-point orifice for this configuration. The stagnation-point pressure was determined from the extrapolation of the pressures around the body and the Newtonian pressure distributions.

Bluff-Afterbody Models

Heat-transfer.- A comparison of the heat transfer in air with that in combustion products for the bluff-afterbody model is shown as the free-stream Stanton number plotted as a function of the position along the model. (See fig. 13.) The heat-transfer coefficient in the Stanton number was based on the total temperature at the model stagnation point, since, for this irregular-shaped body, the local adiabatic wall temperatures were not readily obtainable. The heat transfer on the conical portion of the model is higher for the combustion-products data. The values are slightly higher for the air data near the aft portion of the model, probably because of the previously mentioned small effective angle of attack. The data, however, show that the results obtained in combustion products are in moderately good agreement with those obtained in air.

Figure 14 shows the data obtained in combustion products at an angle of attack of 9.75° and at essentially two values of model stagnation pressure. Data are shown for both the windward and leeward sides of the model. The heat-transfer rate was highest on the cylindrical section on the windward side of the model at the higher model stagnation pressure. The heating rates were generally high over the length of the model on the leeward side at the low value of stagnation pressure. This result could have been caused by the presence of an open wake which persists downstream and permits high-pressure feedback to the model surface, as suggested in reference 7.

Pressure distribution.- The pressure-distribution data along the bluff-afterbody model at an angle of attack of 0° is plotted in the form of pressure coefficient in figure 15. The pressures were determined at a time for which the pressures had reached equilibrium, based on transducer output traces. The local pressures on the conical portion of the model at the higher pressure run are seen to be lower than the free-stream pressure for that condition. The pressure coefficients are generally more positive for the low pressure than for the high-pressure run. This result could also possibly be caused by the wake condition mentioned previously in discussing the heat-transfer results.

The pressure data obtained at an angle of attack of 9.1° are plotted in figure 16. The pressure coefficient on the windward side of the model can be seen to be about the same for the high- and the low-pressure runs. On the leeward side, the low-pressure run had somewhat more positive coefficients than the high-pressure run. Figure 16 shows the pressure coefficients to be much greater on the windward side over the aft portion of the model.

10

CONCLUDING REMARKS

Heat-transfer and pressure-distribution tests were conducted on two different model configurations in methane-air combustion products and in air alone. Data were obtained from combustion products at Mach numbers from 7 to 9, temperatures to 3,100° F, model stagnation pressures from 4 to 14 psia, and stream Reynolds numbers per foot from 0.45×10^6 to 1.1×10^6. Data were obtained in air at a nominal Mach number of 6 at stagnation temperatures from 2,000° F to 2,750° F, at stream Reynolds numbers per foot from 1.6×10^6 to 2.8×10^6, and at model stagnation pressures from approximately 14 to 17 psia.

For the conditions of this investigation, the test results indicate the following:

The experimental heating-rate distribution obtained in combustion products along a hemisphere-cylinder was in good agreement with that obtained in air. Theoretical data were shown to agree reasonably well with the experimental data. The stagnation-point heating rates in air and in combustion products on the hemisphere-cylinder agreed within 10 percent of the theoretical values.

The pressure distributions around a hemisphere-cylinder showed that the results obtained from combustion products were in good agreement with those obtained in air and could be predicted satisfactorily by Newtonian flow theory.

The tests in combustion products of a bluff-afterbody model produced non-dimensional heat-transfer coefficients which were in fair agreement with the results obtained in air.

On the leeward side of a bluff-afterbody model at an angle of attack of about 10°, the heat-transfer and pressure data resulted in higher values at the lower of two Reynolds numbers tested. This result could possibly be attributed to the presence of an open wake in the flow field around the model.

Langley Research Center,
National Aeronautics and Space Administration,
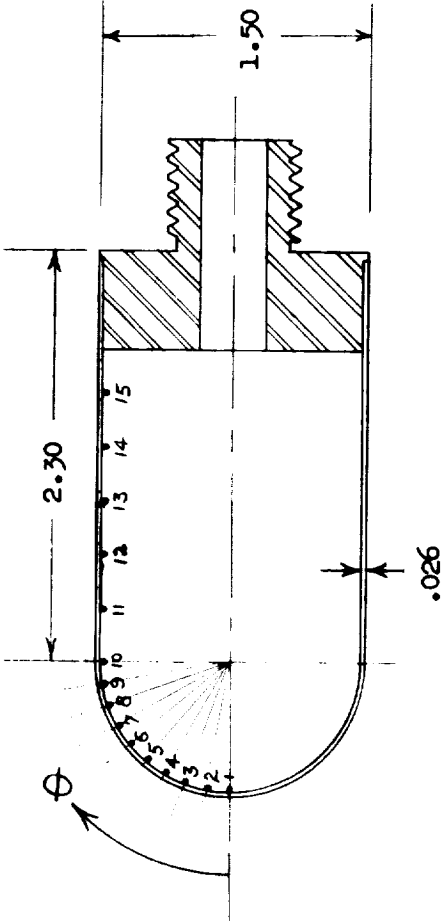Langley Station, Hampton, Va., August 17, 1962.

REFERENCES

1. Trout, Otto F., Jr.: Experimental Investigation of Several Copper and Beryllium Hemispherical Models in Air at Stagnation Temperatures of 2,000° F to 3,600° F. NASA TM X-55, 1959.

2. Crawford, Davis H., and McCauley, William D.: Investigation of the Laminar Aerodynamic Heat-Transfer Characteristics of a Hemisphere-Cylinder in the Langley 11-Inch Hypersonic Tunnel at a Mach Number of 6.8. NACA Rep. 1323, 1957. (Supersedes NACA TN 3706.)

3. Crawford, Davis H.: Investigation of the Flow Over a Spiked-Nose Hemisphere-Cylinder at a Mach Number of 6.8. NASA TN D-118, 1959.

4. Leyhe, E. W., and Howell, R. R.: Calculation Procedure for Thermodynamic, Transport, and Flow Properties of the Combustion Products of a Hydrocarbon Fuel Mixture Burned in Air With Results for Ethylene-Air and Methane-Air Mixtures. NASA TN D-914, 1962.

5. Fay, J. A., and Riddell, F. R.: Theory of Stagnation Point Heat Transfer in Dissociated Air. Jour. Aero. Sci., vol. 25, no. 2, Feb. 1958, pp. 73-85, 121.

6. Kemp, Nelson H., Rose, Peter H., and Detra, Ralph W.: Laminar Heat Transfer Around Blunt Bodies in Dissociated Air. Jour. Aero/Space Sci., vol. 26, no. 7, July 1959, pp. 421-430.

7. Thomas, R. E., and Lee, J. D.: The Ohio State University 12-Inch Hypersonic Wind Tunnel System. Rep. No. TN(ALOSU)559-2 (WADC TN 59-280), Ohio State Univ. Res. Foundation, July 1959.

TABLE I.- STAGNATION-POINT HEAT-TRANSFER DATA FOR HEMISPHERE-CYLINDER

Test	T_s, °R	T_o, °R	p_t, psia	p_s, psia	Experimental h_s, Btu/ft²-sec-°R	Experimental $q_{c,s}$, Btu/ft²-sec	M_∞
Combustion products							
1	3,310	575	1,609	5.95	0.0286	78.1	8.7
2	3,220	590	1,670	6.17	.0283	74.3	8.8
3	2,985	580	1,663	6.15	.0252	60.5	8.9
4	2,550	575	1,014	3.75	.0197	39.2	9.2
5	3,115	580	1,766	6.53	.0275	69.7	8.8
6	2,960	560	2,147	7.94	.0289	69.3	8.9
7	3,100	575	1,369	5.06	.0266	67.2	8.8
8	3,240	610	1,068	3.95	.0261	68.7	8.7
9	3,100	600	1,109	4.10	.0289	72.3	8.8
10	3,005	570	960	3.55	.0236	57.6	8.8
11	2,995	575	1,408	5.20	.0251	60.8	8.9
12	3,380	565	1,405	8.85	.0385	108.5	7.6
13	3,340	560	1,450	9.15	.0385	106.9	7.7
14	3,215	565	1,560	9.84	.0347	91.9	7.8
15	3,390	550	975	8.50	.0360	102.4	7.1
16	3,390	560	960	8.35	.0342	96.8	7.1
Air							
1	2,420	910	732	17.00	0.0447	67.5	6.4
2	3,210	925	738	13.95	.0401	91.6	6.2

THERMOCOUPLE LOCATIONS

Thermo-couple	θ, deg	Distance aft of hemisphere-cylinder juncture, in.
1	0	
2	10	
3	20	
4	30	
5	40	
6	50	
7	60	
8	70	
9	80	
10	90	0.0
11		.3
12		.6
13		.9
14		1.2
15		1.5

(a) Heat-transfer model.

Figure 1.- Details of heat-transfer and pressure-distribution hemisphere-cylinder models.

PRESSURE-ORIFICE LOCATIONS

Orifice number	ϕ, deg	β, deg	Distance aft of hemisphere-cylinder juncture, in.
1	0	0	
2	10	40	
3	20	80	
4	30	120	
5	40	160	
6	50	200	0.0
7	60	240	
8	70	280	
9	80	320	
10	90	360	
11	40	340	
12		30	.375
13		60	.750
14		90	1.125
15		120	1.500

(b) Pressure-distribution model.

Figure 1.- Concluded.

15
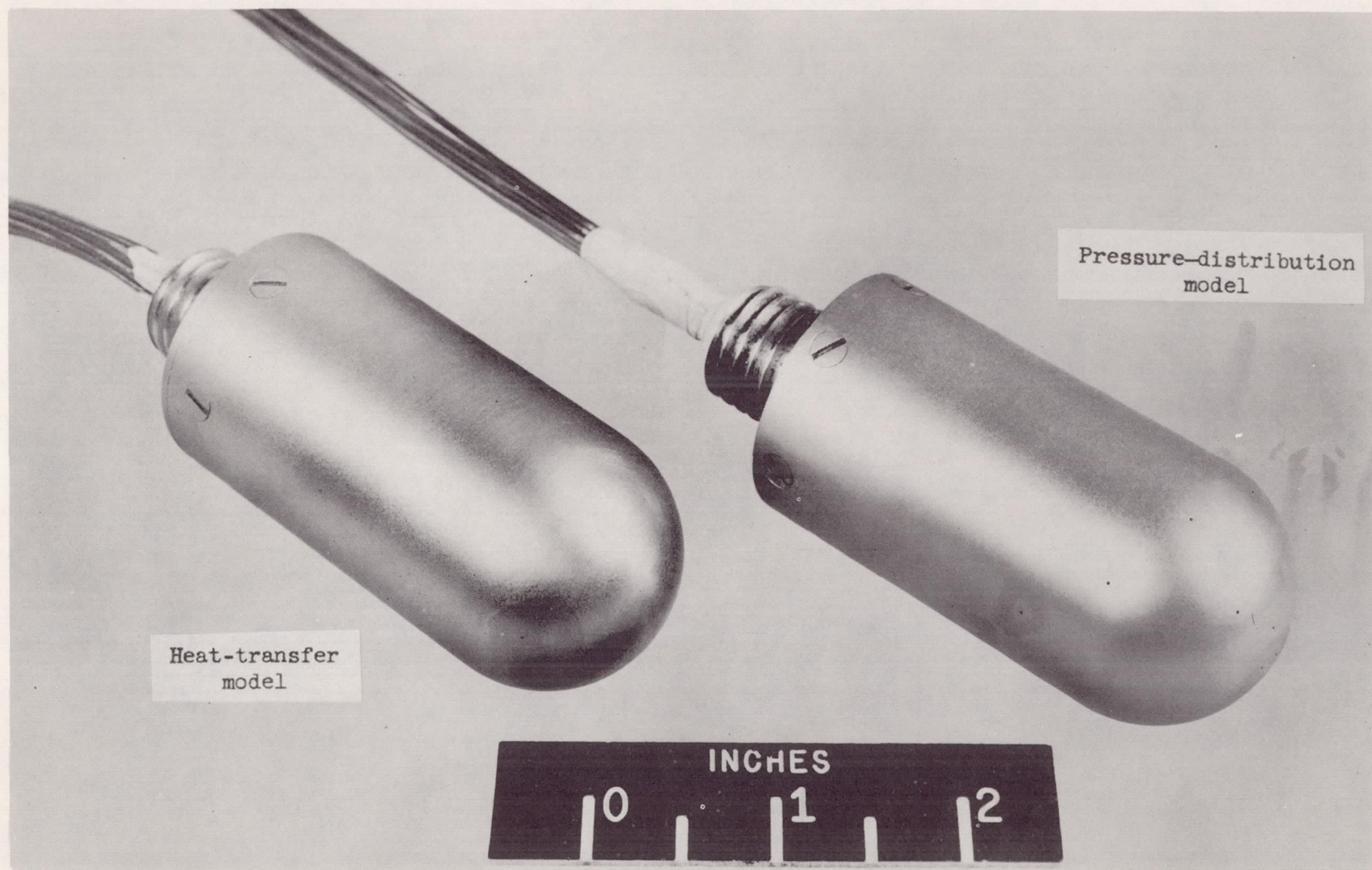
L-60-2731.1

Figure 2.- Photograph of heat-transfer and pressure-distribution hemisphere-cylinder models.
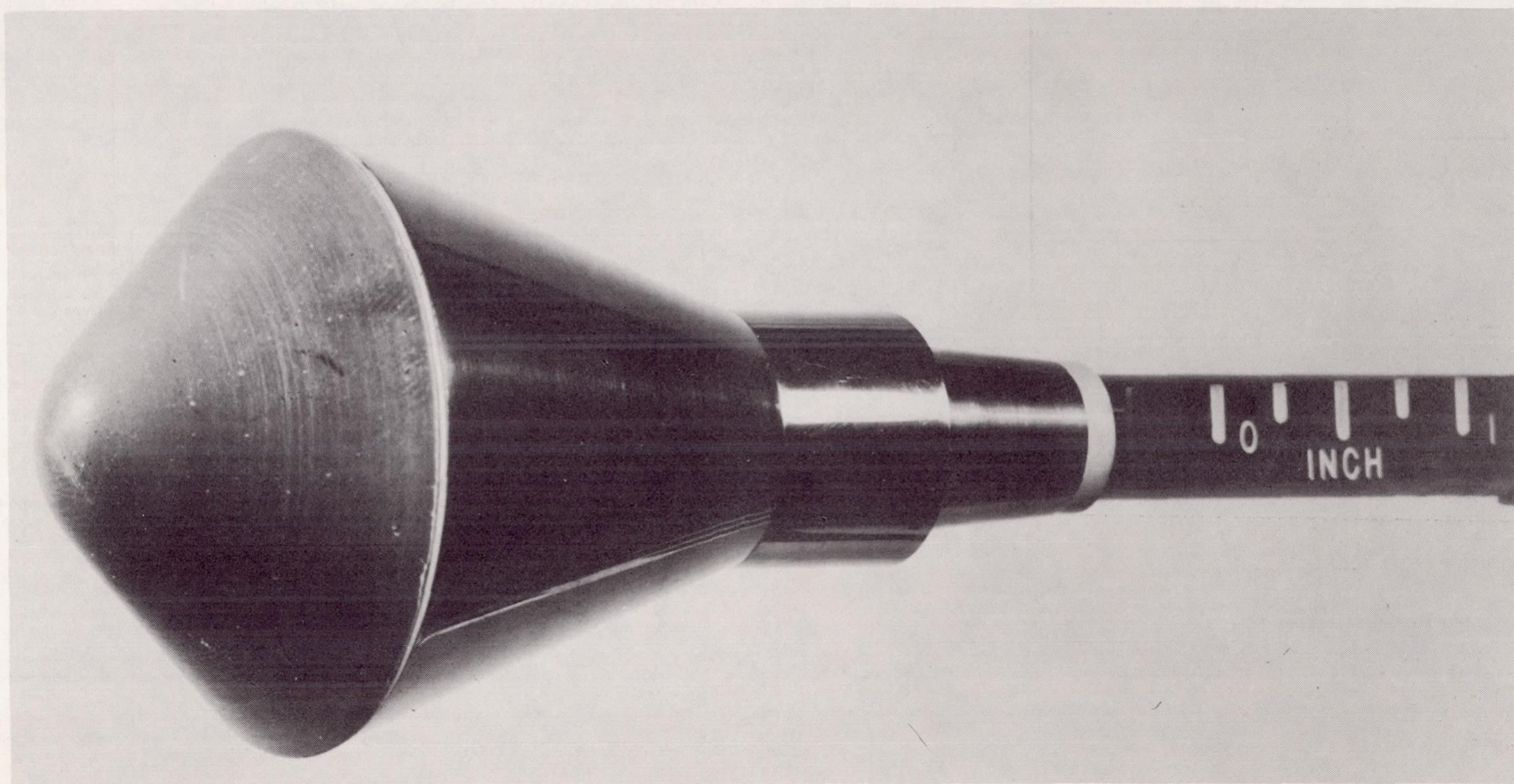
Figure 3.- Photograph of bluff-afterbody heat-transfer model.   L-61-5247

Thermo-couple	s/D	Wall Thickness, in.
1	0.210	0.0105
2	.316	.0105
3	.423	.0105
4	.529	.0105
5	.636	.0110
6	.689	.0110
7	.742	.0110
8	.795	.0110
9	.846	.0110
10	.896	.0110
11	.946	.0105
12	.996	.0105
13	1.046	.0105
14	1.096	.0105
15	1.130	.0100
16	1.146	.0100
17	1.196	.0100
18	1.246	.0100
19	1.296	.0100
20	1.346	.0100
21	1.396	.0100

(a) Heat-transfer model.

Figure 4.- Details of heat-transfer and pressure-distribution bluff-afterbody models. Dimensions in inches.

Orifice	s/D
1	0.115
2	.233
3	.527
4	.644
5	.762
6	.810
7	.885
8	1.002
9	1.078
10	1.128
11	1.319
12	1.393

(b) Pressure-distribution model.

Figure 4.- Concluded.

Test-section housing

Test section

Supersonic
diffuser

Axisymmetric
nozzle

Model
support
strut

Model pitch cylinder

Nozzle film
injection
slot

Combustion
chamber
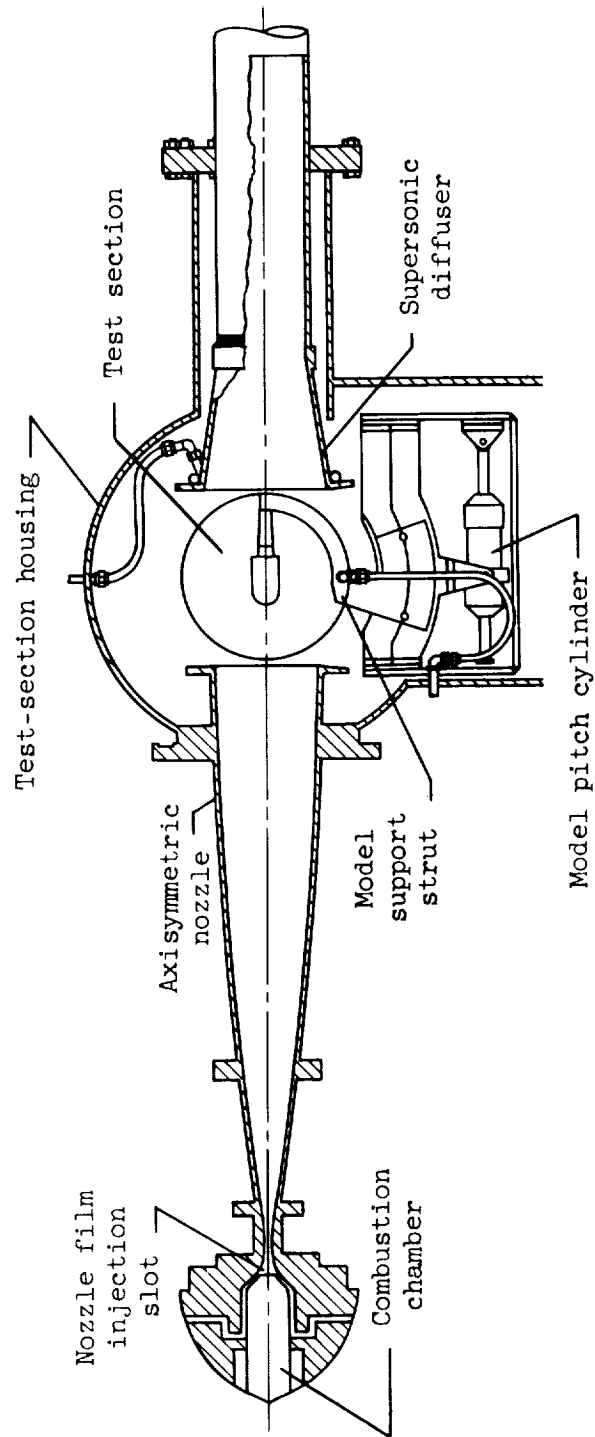
Figure 5.- Nozzle and test section of the 7-inch Mach 7 pilot tunnel at Langley Research Center.
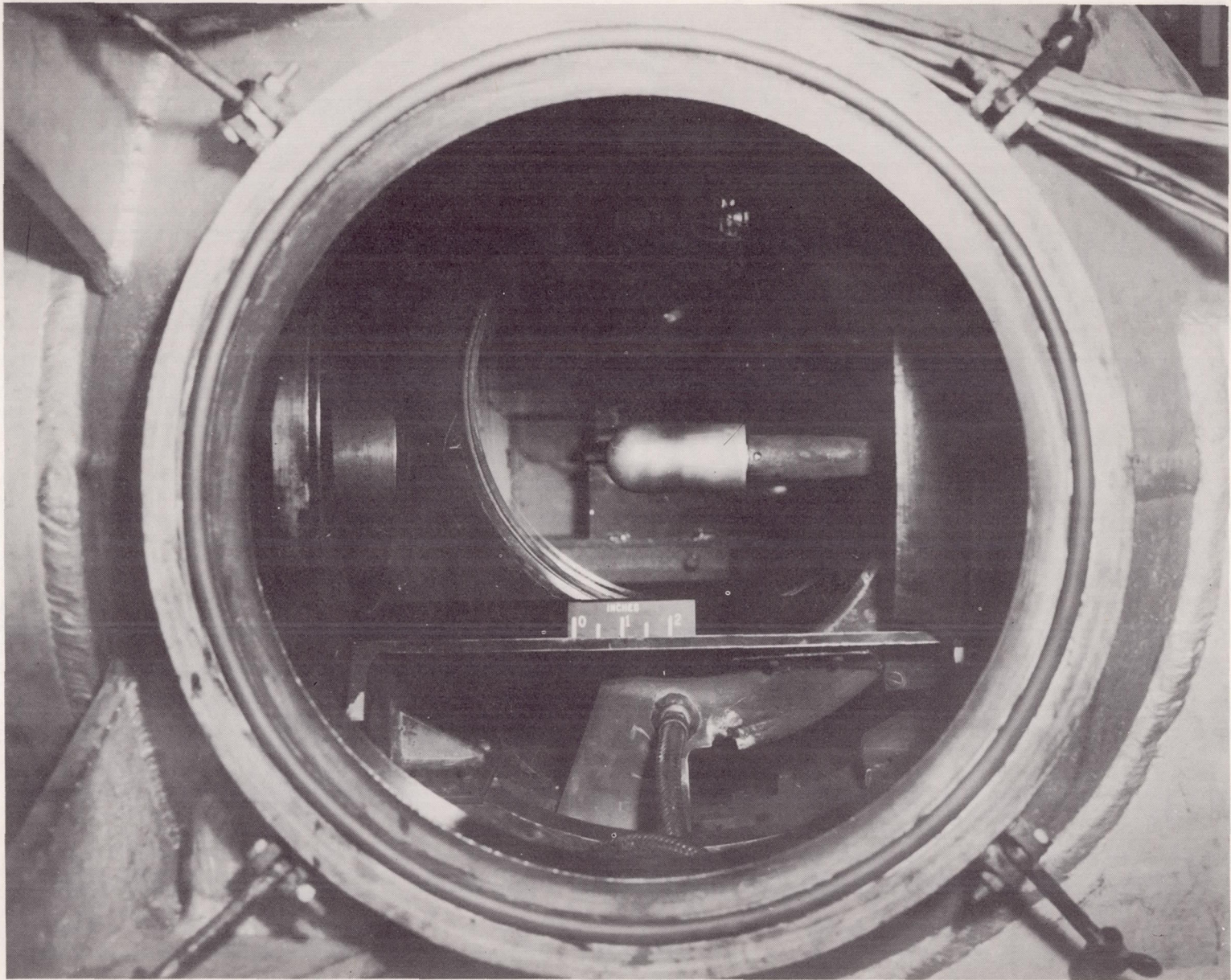
L-61-4017

Figure 6.- Hemisphere-cylinder model in test section of 7-inch Mach 7 pilot tunnel at Langley Research Center.
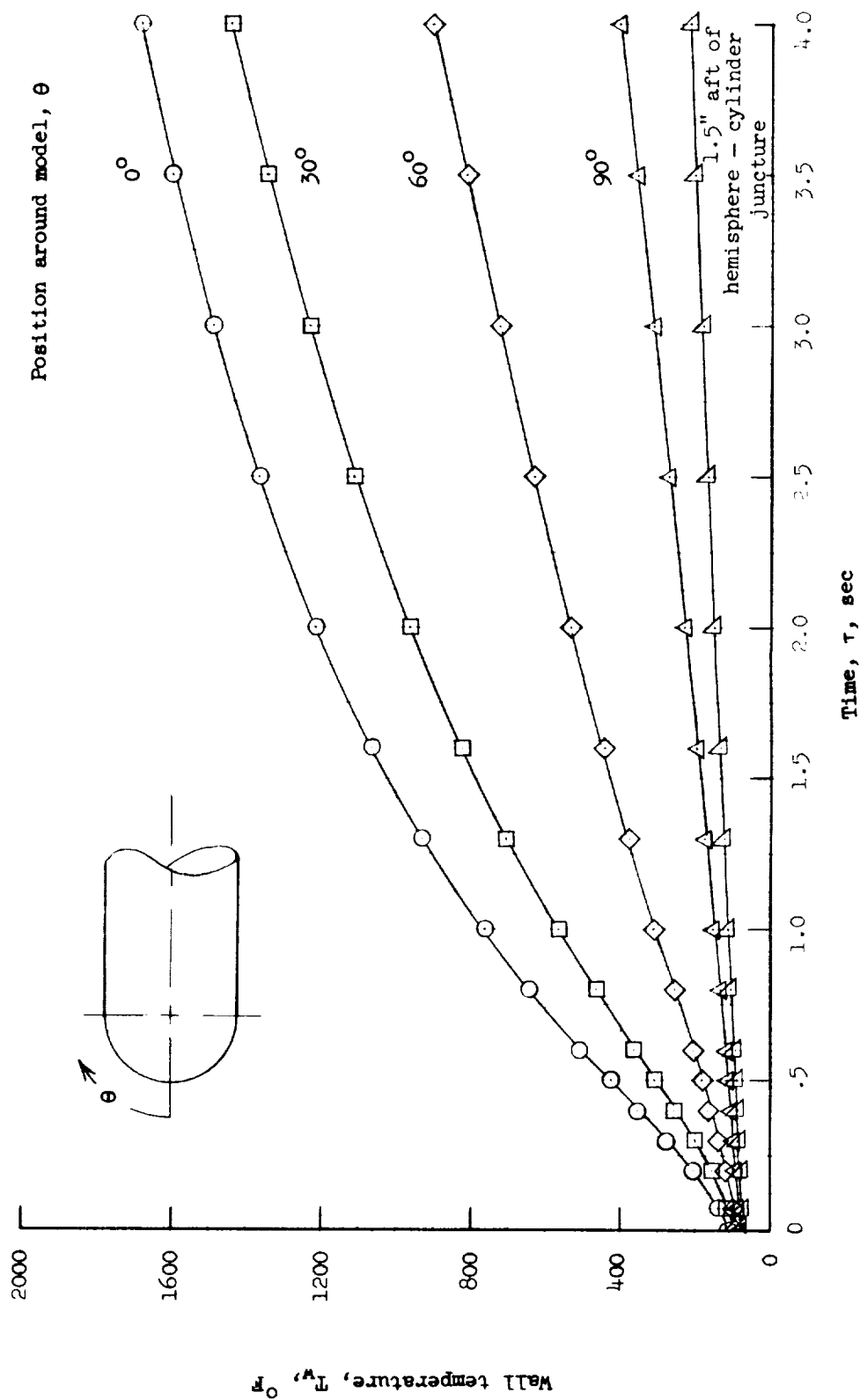
Figure 7.- Typical temperature-time history at several positions on hemisphere-cylinder model.
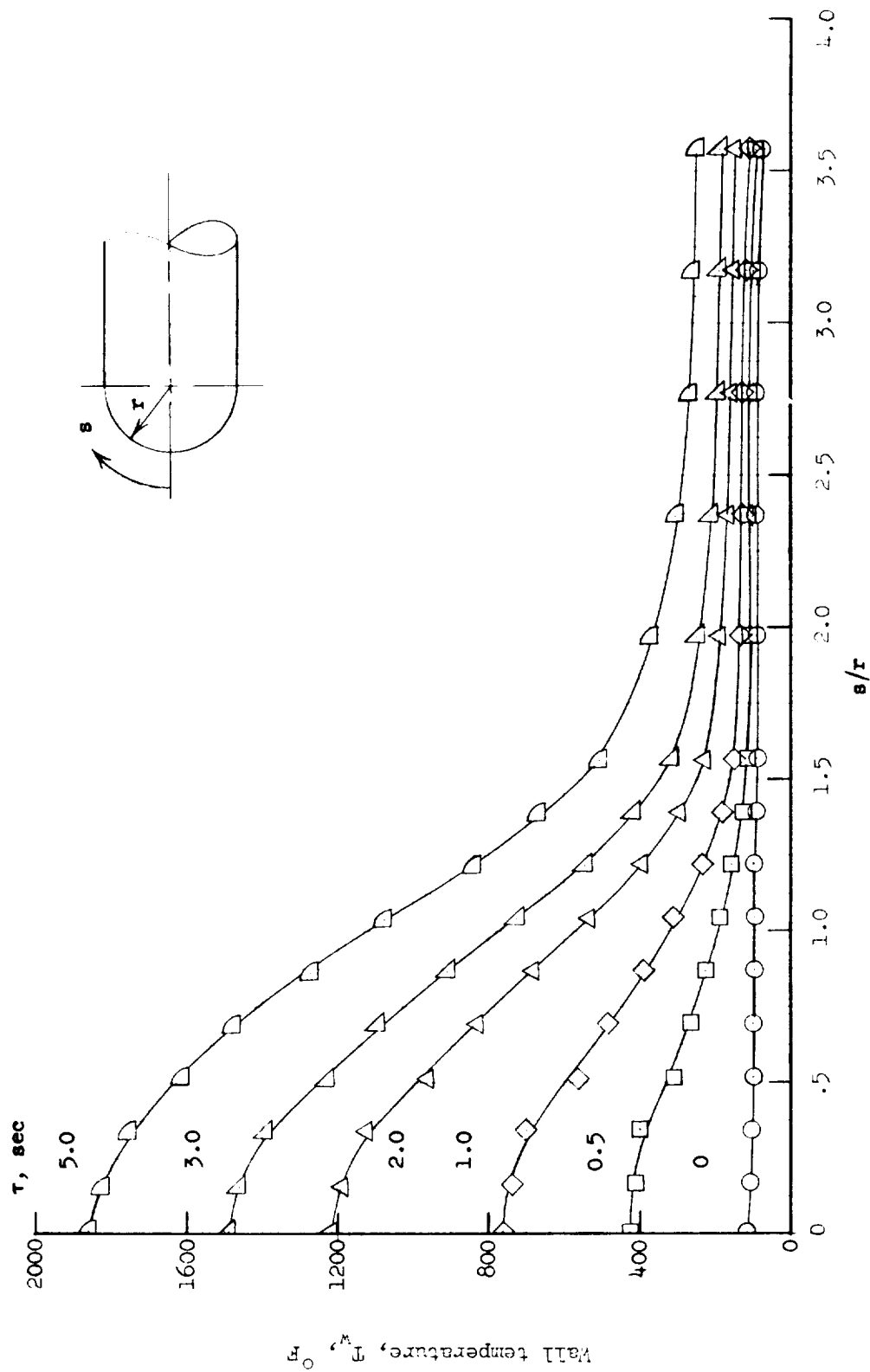
Figure 8.- Temperature distribution along hemisphere-cylinder for several increments of time.
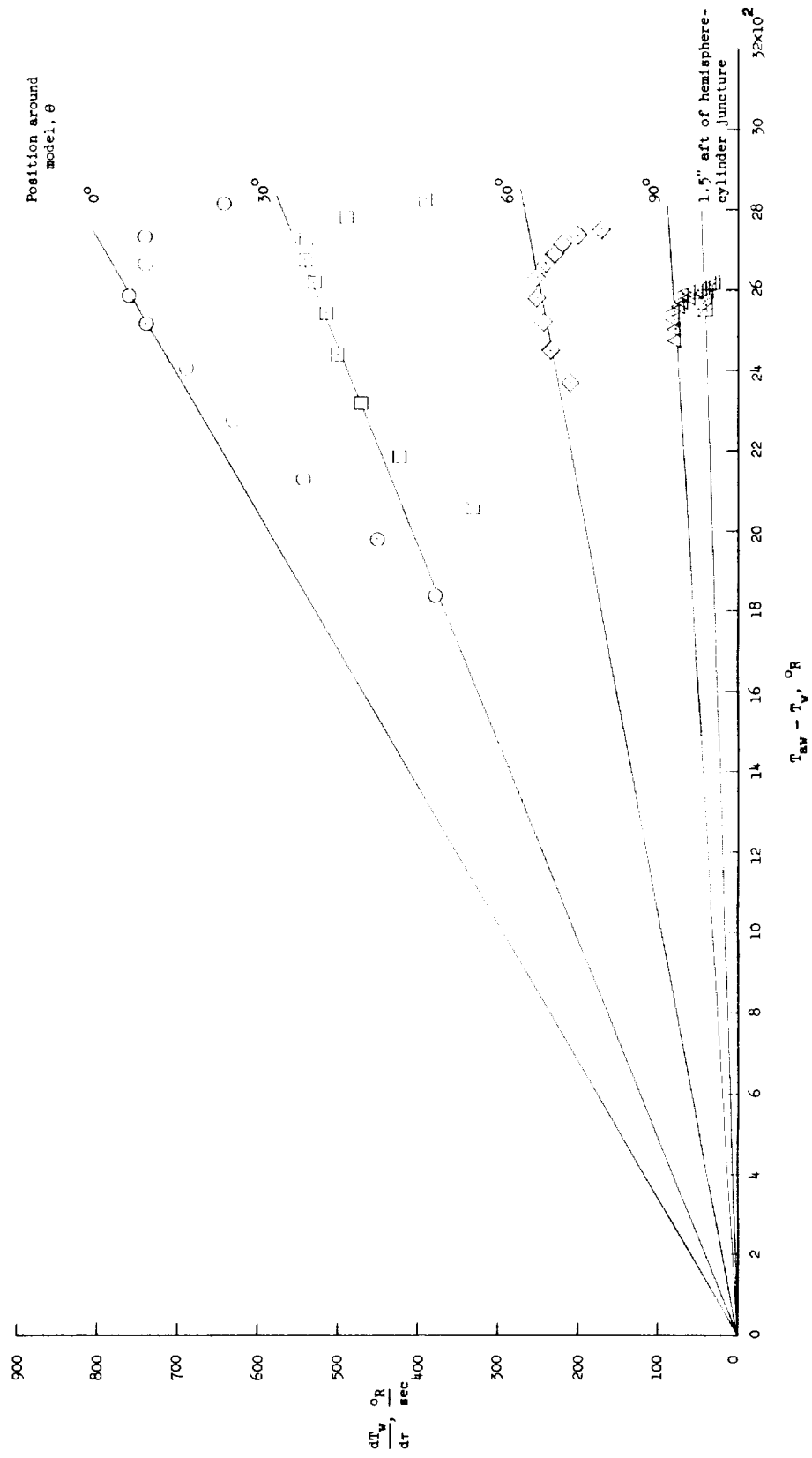
Figure 9.— Temperature-time slopes plotted against difference between adiabatic and actual wall temperatures for a typical test run on hemisphere-cylinder model.
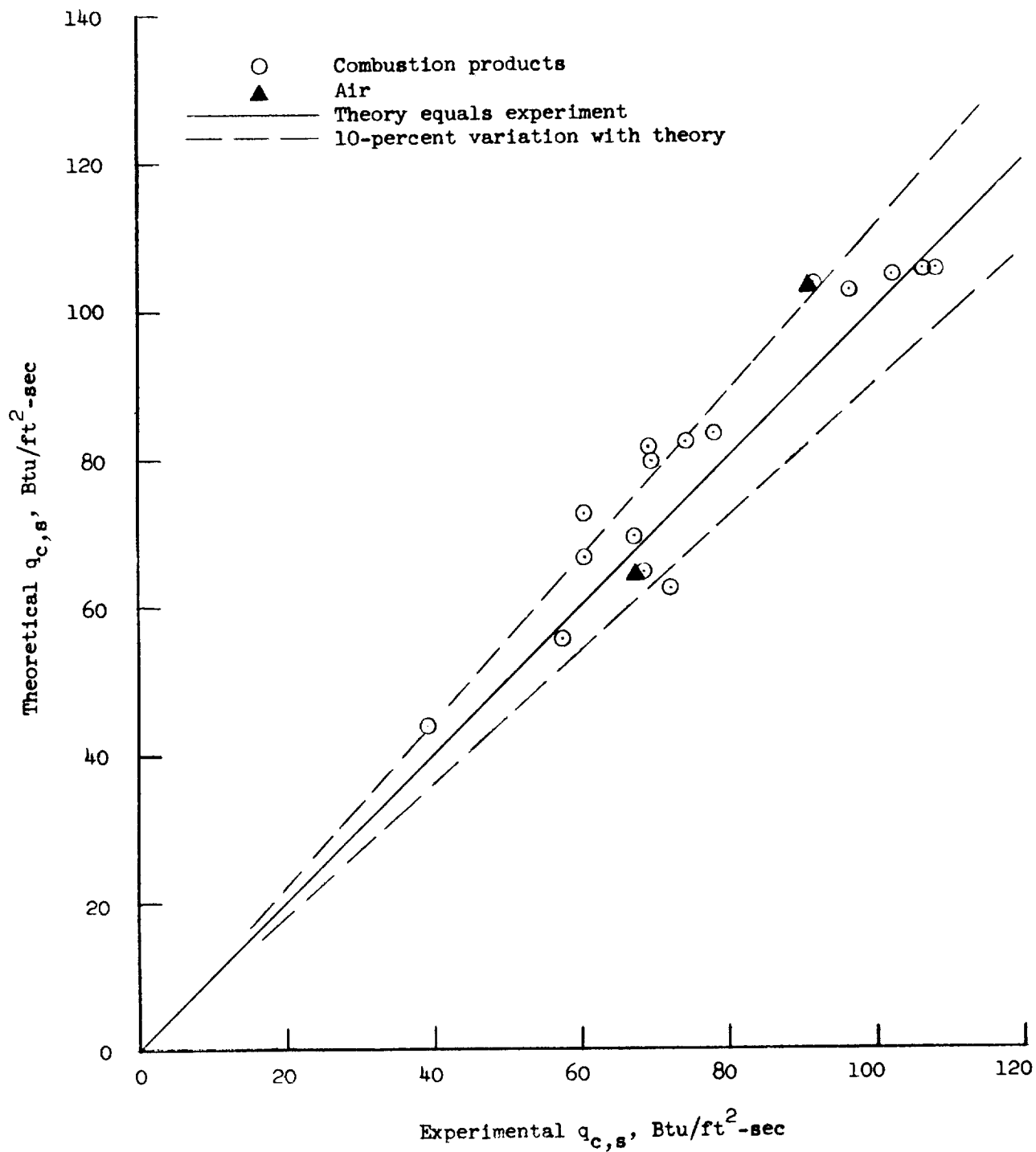
Figure 10.- Comparison of theoretical and experimental stagnation-point heating rates on hemisphere-cylinder.
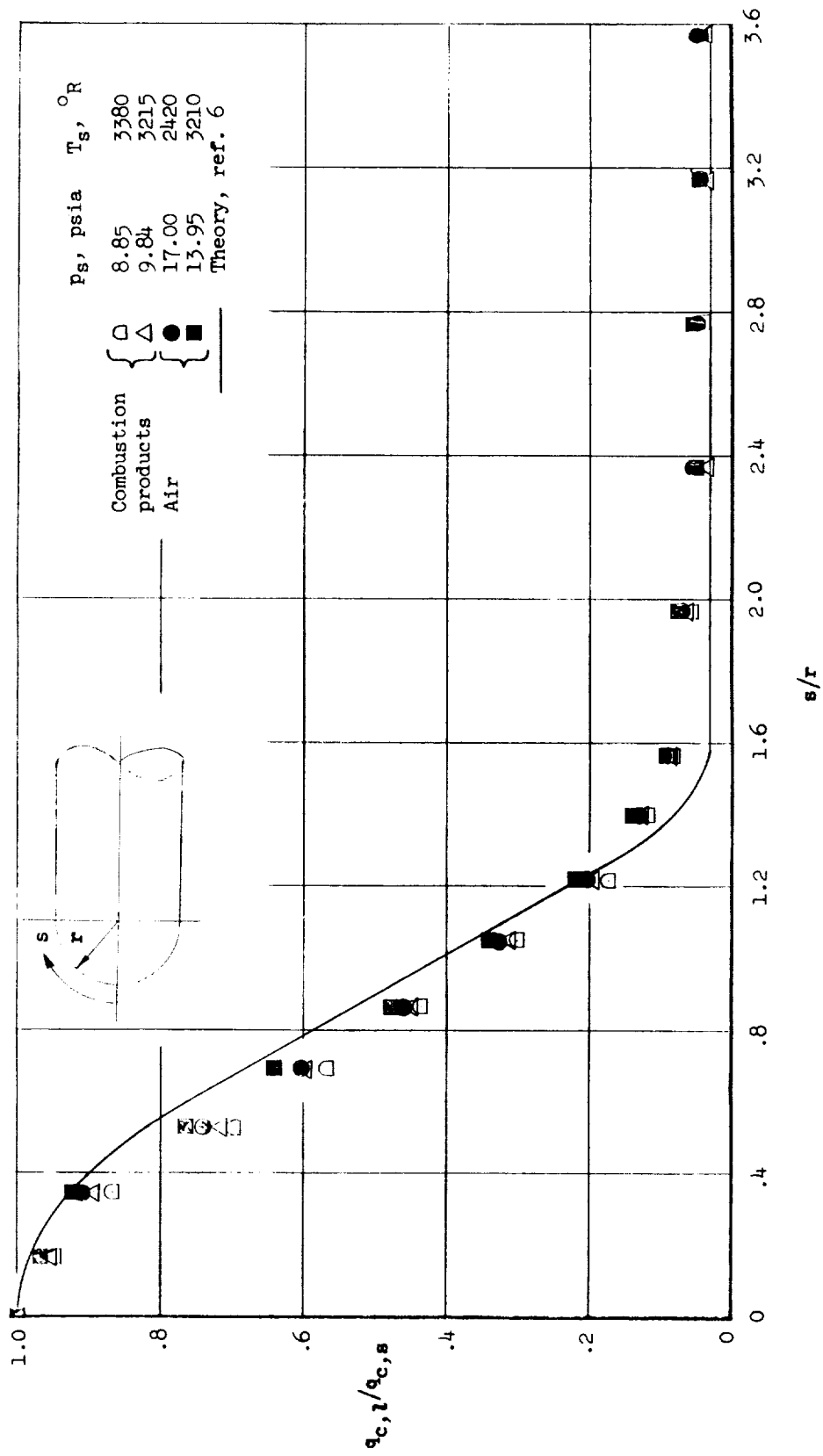
Figure 11.- Heat-transfer distribution along hemisphere-cylinder models.
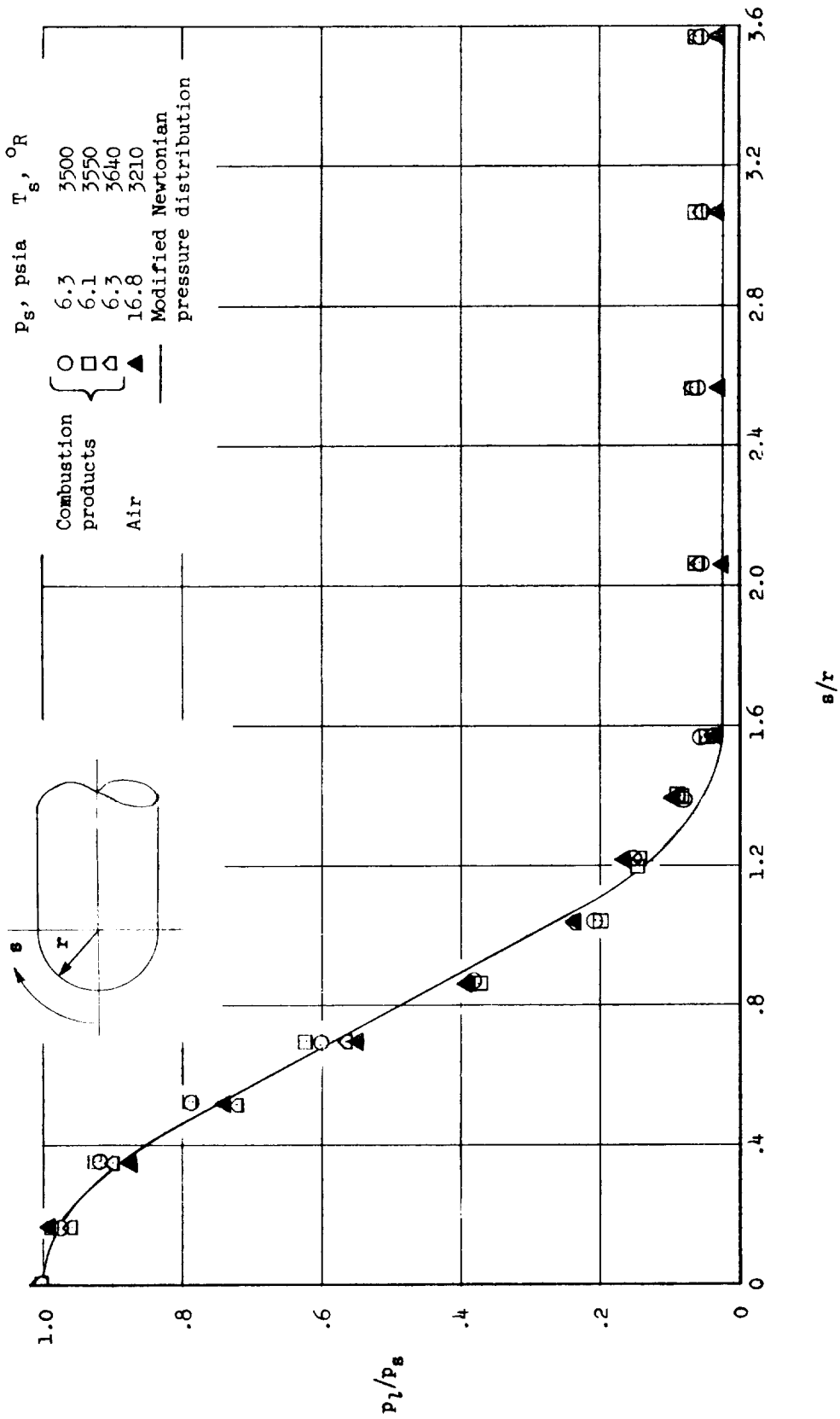
Figure 12.- Pressure distribution along hemisphere-cylinder models.
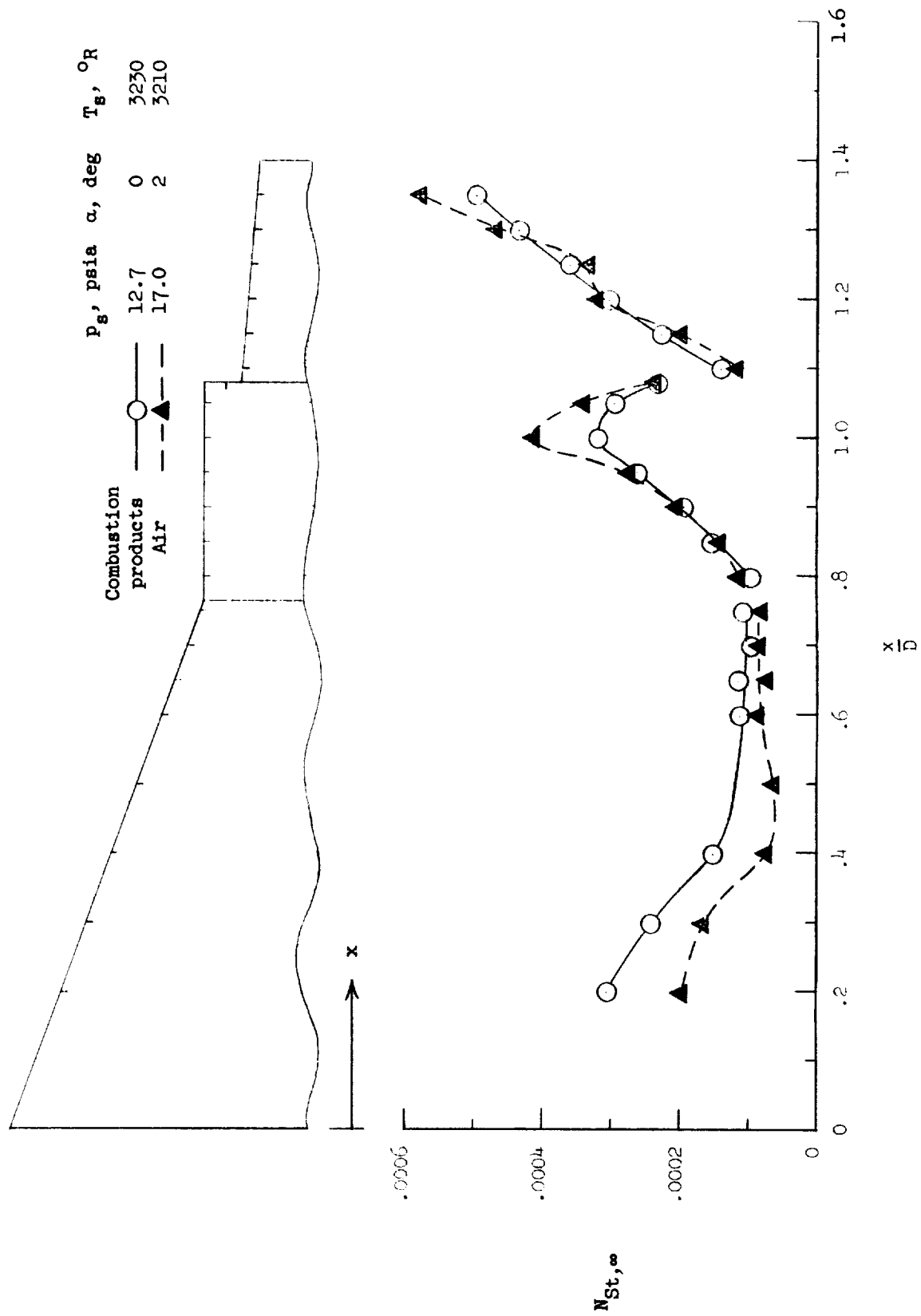
Figure 13.- Comparison of heat transfer in air with that in combustion products on bluff-afterbody model.
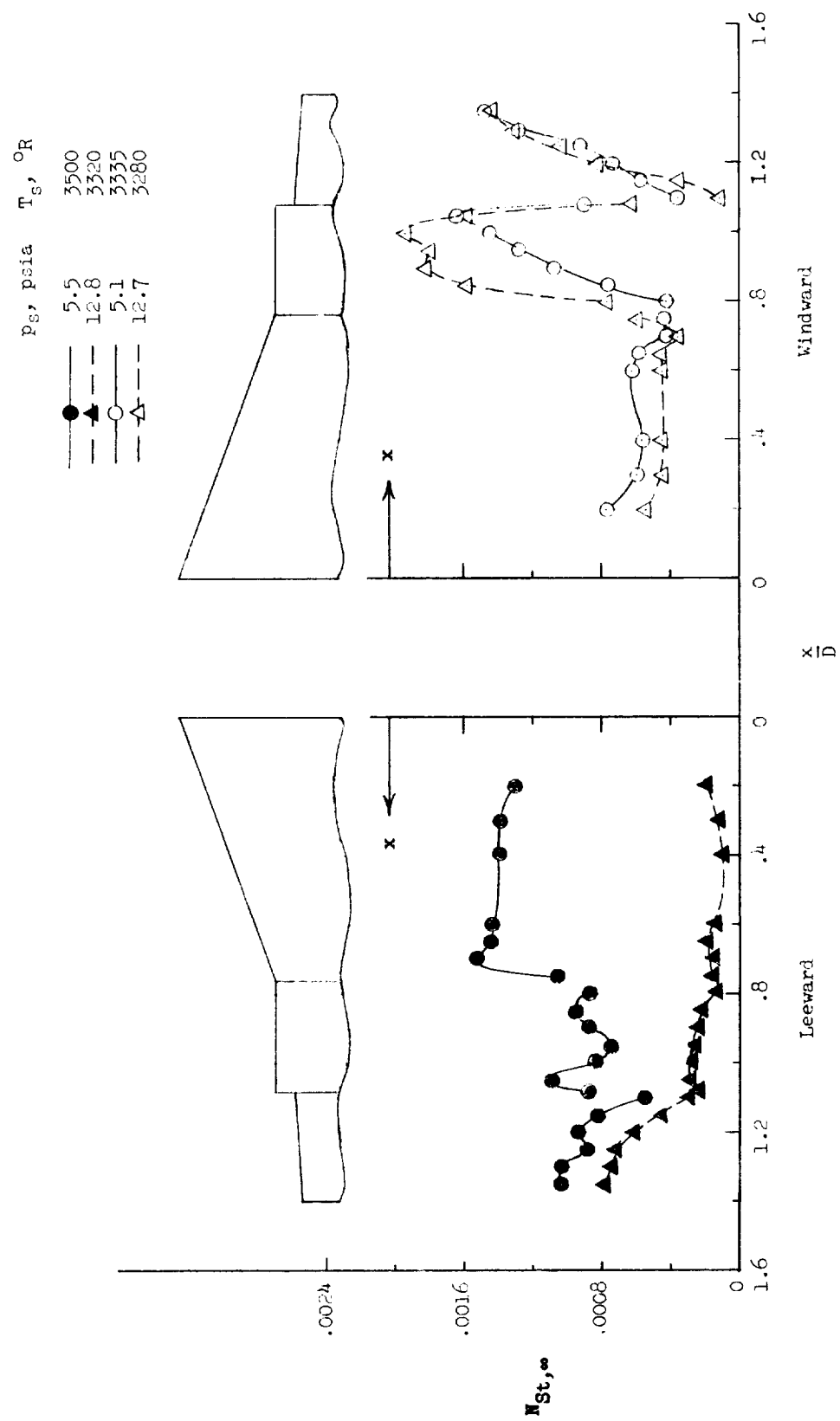
28

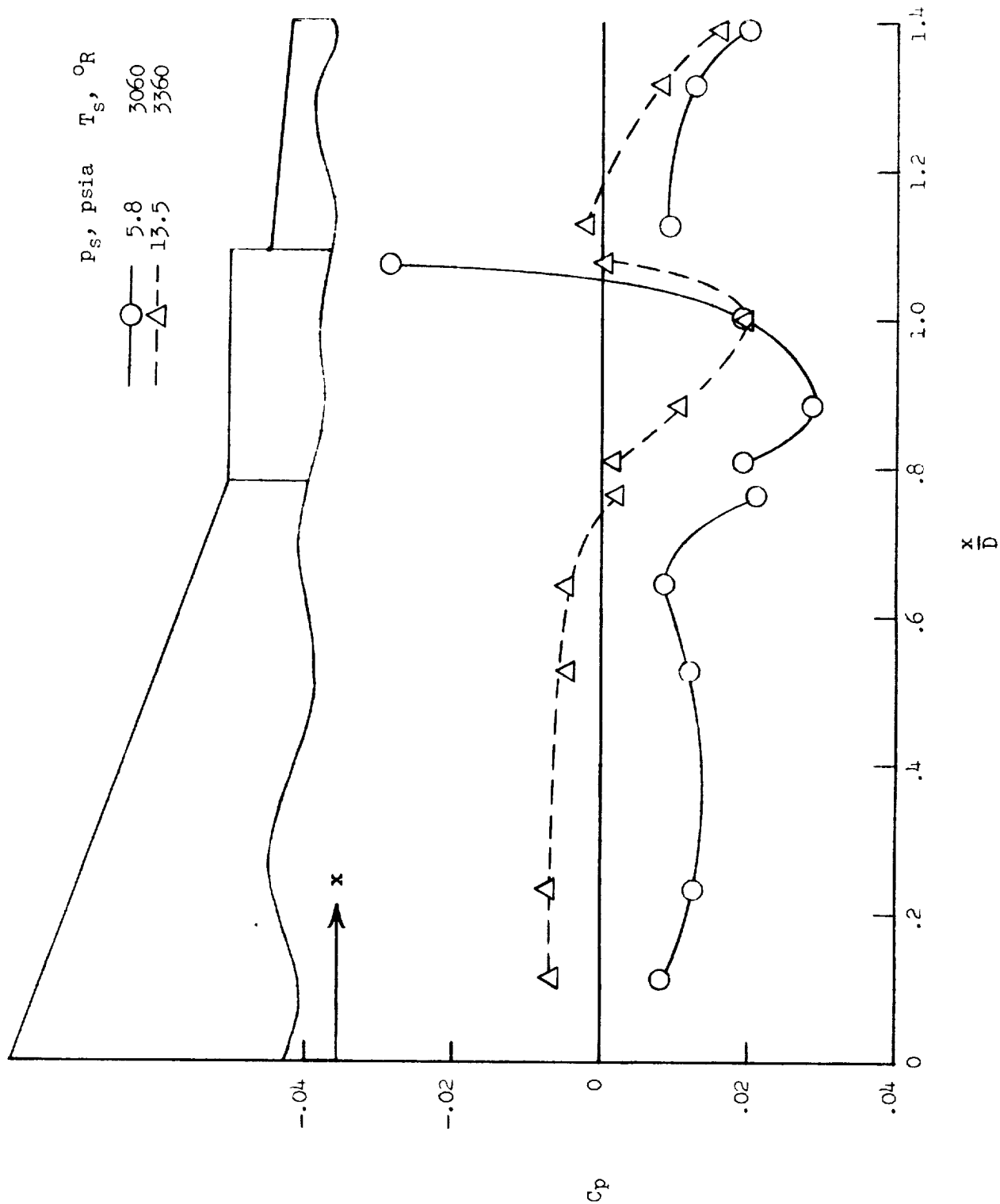Figure 14.- Heat-transfer data along bluff-afterbody model in combustion products. $\alpha = 9.75°$.

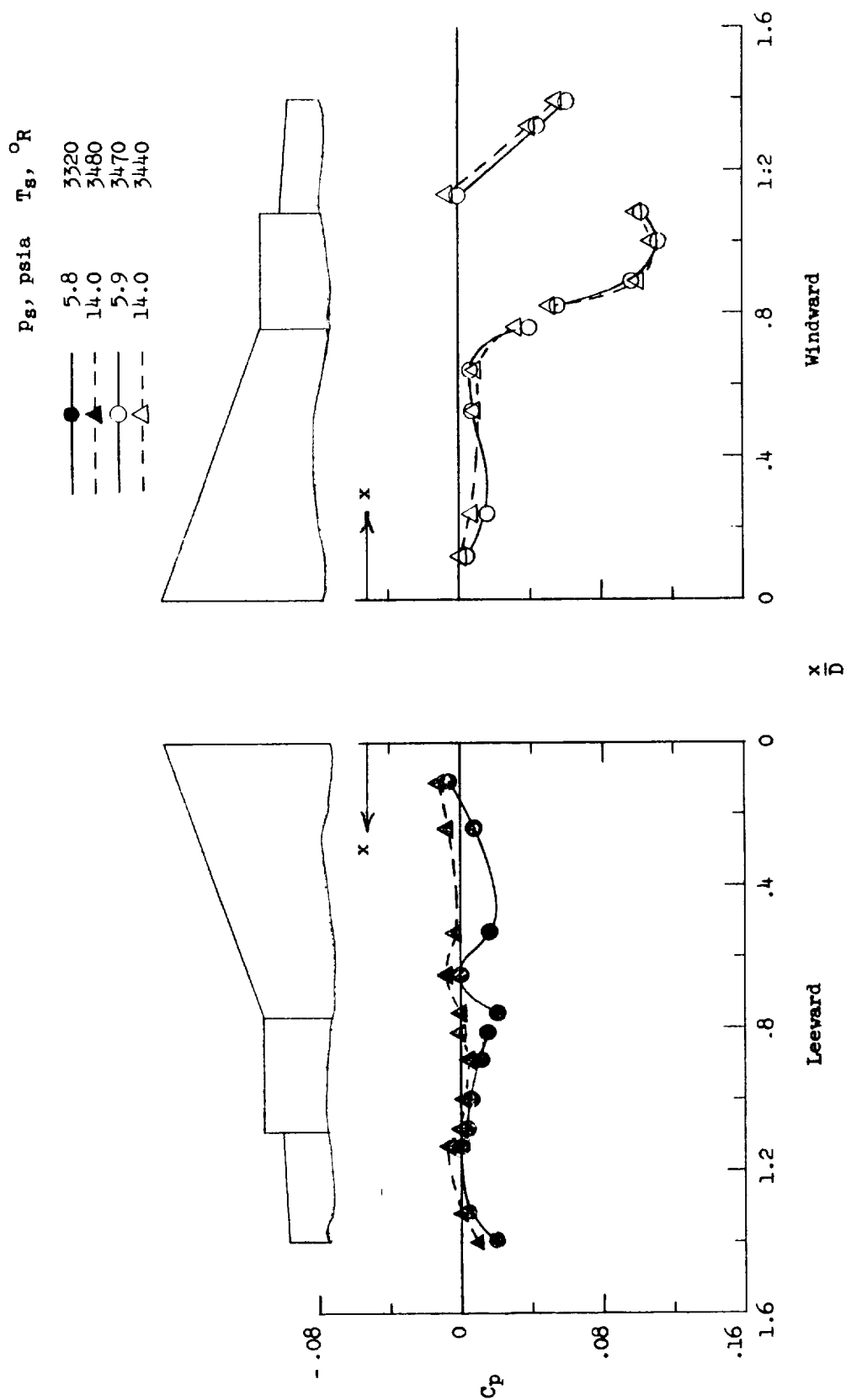Figure 15.- Variation of pressure coefficient along model. $\alpha = 0°$.

Figure 16.- Variation of pressure coefficient along model. $\alpha = 9.1^{\circ}$.